Resistive Wall Mode Active Stabilization in High Beta, Low Rotation Plasmas

S.A. Sabbagh 1), R.E. Bell 2), J.E. Menard 2), D.A. Gates 2), A.C. Sontag 1), J.M. Bialek 1), B.P. LeBlanc 2), F.M. Levinton 3), K. Tritz 4), H. Yuh 3)

1) Department of Applied Physics and Applied Mathematics, Columbia University, New York, NY, USA
2) Princeton Plasma Physics Laboratory, Princeton University, Princeton, NJ, USA
3) Nova Photonics, Princeton, NJ, USA
4) Johns Hopkins University, Baltimore, MD, USA

e-mail contact of main author: sabbagh@pppl.gov

Abstract. In recent experiments, the resistive wall mode was actively stabilized in the National Spherical Torus Experiment in high beta plasmas rotating significantly below the critical rotation speed for passive stability and in the range predicted for the International Thermonuclear Experimental Reactor (ITER). [1] Variation of feedback stabilization parameters showed mode excitation or suppression. Stabilization of toroidal mode number unity did not lead to instability of toroidal mode number two. The mode can become unstable by deforming poloidally, an important consideration for stabilization system design.

1. Introduction

Large scale magnetohydrodynamic (MHD) instabilities impose significant limits to fusion power production in magnetic fusion plasmas. A basic, yet formidable example is the long wavelength kink-ballooning instability which grows on the rapid Alfvén timescale and typically leads to plasma pressure collapse and current disruption. This mode rotates along with a rotating plasma and may be stabilized by the presence of an electrically conducting wall, but also results in the potential destabilization of the resistive wall mode (RWM) [2,3], a branch of the kink instability that grows on the relatively slow eddy current decay time of the resistive wall, τ_w. The RWM is amenable to passive stabilization [4,5,2] whether or not the mode rotates with respect to the conducting wall, and theoretically occurs due to energy dissipation related to plasma rotation [6,7]. At sufficiently high plasma pressure in relation to the confining magnetic field, (toroidal and normalized plasma beta, $\beta_t \equiv 2\mu_0\langle p\rangle/B_0^2$ and $\beta_N \equiv 10^8\langle\beta_t\rangle aB_0/I_p$,) and at plasma toroidal rotation speeds, ω_ϕ, below a critical value, Ω_{crit}, the RWM becomes unstable, typically leading to plasma disruption within a few τ_w. Here, p is the plasma pressure, B_0 is the vacuum toroidal field at the plasma geometric center, a is the plasma minor radius at the midplane, I_p is the plasma current, and brackets represent volume average. In both theory and experiment, RWM destabilization can occur when β_N exceeds $\beta_{N(n)}^{no\text{-}wall}$, the value where ideal MHD modes become unstable for the toroidal mode number, n, of interest with no stabilizing wall present. In this paper, $\beta_N^{no\text{-}wall} = \beta_{N(n=1)}^{no\text{-}wall}$. The critical rotation speed is usually quoted at low integer values of the plasma safety factor, q, (typically, q = 2) normalized to the Alfvén frequency, ω_A, and Ω_{crit}/ω_A is typically one to a few percent [8,9]. Generally, the larger plasma rotation profile is important in determining RWM stability [5,9,10]. Therefore, Ω_{crit} is more appropriately expressed as a profile, rather than a scalar. [11] Experimental comparison of similar plasmas created in the DIII-D and NSTX devices also shows that Ω_{crit}/ω_A is dependent on the aspect ratio of the device $A \equiv R_0/a$, where R_0 is the major radius [10]. Confirmation of RWM passive stabilization physics is still an active area of research.

RWM active stabilization can be used when the plasma rotation is insufficient for RWM passive stabilization and is expected to be required for burning fusion plasmas in the International Thermonuclear Experimental Reactor (ITER) [12] operating in high performance scenarios [9]. Active stabilization has been addressed to stabilize pressure-driven modes in rotating tokamak plasmas [13-15] and current-driven modes in reversed-field pinches [16]. Since $\omega_\phi / \Omega_{crit}$ is expected to be less than unity in ITER and other future burning plasma experiments, present tokamak research now focuses on active stabilization of the n = 1 RWM at these low levels of ω_ϕ [15]. Stabilization is typically realized by a feedback control loop consisting of magnetic sensors capable of detecting the spectrum of low frequency ~ O($1/\tau_w$) magnetic perturbations, a set of control coils to provide magnetic field in response to the detected magnetic perturbations, and a control algorithm that determines the form of the response. Control algorithms aim to approximately eliminate the dominant measured field asymmetry [17], produced by some combination of the RWM and eddy currents induced by the mode flowing in nearby conducting structure. Tokamak experiments presently focus on stabilizing RWMs with n = 1 since they minimize field line bending and are usually the least stable. Important corollary research includes how the RWM reacts to stabilization, including the behavior of $n > 1$ modes in this condition.

2. RWM Active Stabilization of Low Rotation Plasmas

The present study demonstrates for the first time active stabilization of the pressure-driven RWM in high beta, low aspect ratio tokamak plasmas, with ω_ϕ significantly below the entire critical rotation profile. The low A configuration, or spherical torus [18], produces a high β_t operating regime and plasmas with the highest energy confinement, τ_E, operate in advanced tokamak states with broad pressure and current (low plasma internal inductance, l_i) equilibrium profiles. These conditions are most amenable to kink and RWM passive and active stabilization. The experiments were performed in the National Spherical Torus Experiment (NSTX) [19], recently outfitted with an active RWM stabilization system. Current ramping to decrease l_i, or other techniques to reduce $\beta_N^{no\text{-}wall}$ used to excite RWM growth in tokamaks [14], were not required. The role of the n = 2 RWM during active n = 1 RWM stabilization can be readily studied, since the device is equipped to measure up to n = 3, and unstable RWMs with n = 1 – 3 have already been observed in NSTX [5]. Plasma rotation is measured at 51 major radial locations at the device midplane by a charge exchange recombination spectroscopy diagnostic using emission from C^{5+} at 5290Å. Toroidally-directed neutral beam injection power, P_b, used to heat the plasma normally produces high plasma rotation, that has reached values of $\omega_\phi/\omega_A = 0.48$ [5]. Plasma toroidal rotation was controlled in these experiments by the application of non-resonant, n = 3 magnetic braking [20], reducing ω_ϕ significantly below Ω_{crit}, and in the predicted range of $\omega_\phi / \Omega_{crit}$ for ITER plasmas. The present results have important ramifications for the design of RWM stabilization systems planned for future devices such as ITER and the Korean Superconducting Tokamak Advanced Research device (KSTAR) [21].

A comparison of high β_N plasmas with and without RWM active stabilization is shown in FIG. 1 where n = 3 braking fields were applied to slow ω_ϕ below Ω_{crit}. All discharges have constant neutral beam power, P_b = 6.3MW. The plasma without active stabilization (dashed curves) reaches β_N = 4.1 as $\omega_\phi/2\pi$ at major radial position R = 1.323m drops to below 4 kHz. This radial position is chosen since it is near the q = 2 flux surface. At this time, RWM passive stabilization becomes insufficient and the n = 1 RWM becomes unstable, indicated by poloidal and radial field sensors (ΔB_p, $\Delta B_{r\text{-ext}}$), and β_N collapses. With active stabilization turned off, the current in one of three control coil pairs, I_A, is the pre-programmed n = 3 braking field current (FIG. 1(c)). The experimentally fitted n = 1 RWM growth rate is between 0.5 – 0.25 s^{-1}. This agrees well with the theoretical growth rate of 0.37 s^{-1} as computed by the VALEN-3D code [22], using experimental plasma equilibrium reconstructions [23] including internal magnetic field pitch angle constraints from a motional Stark effect diagnostic. This value is used as the RWM growth rate, γ_{RWM}, in this paper. In contrast, the plasma with active stabilization (solid curves) does not suffer an unstable RWM and continues to increase in β_N up to 5.6 and β_t up to 19.4%, as ω_ϕ continues to decrease to $\omega_\phi/\Omega_{crit}$ = 0.2 near q = 2 before the end of the discharge. The RWM is actively stabilized above $\beta_N^{no\text{-}wall}$ and below Ω_{crit} for significantly long duration exceeding 90/γ_{RWM} and seven τ_E. The time evolution of $\beta_N^{no\text{-}wall}$ is computed by the DCON MHD stability code [24] using experimental equilibrium reconstructions. The control coil current is now the superposition of n = 3 braking field current and n = 1 active feedback stabilization current which is determined by the measured n = 1 RWM amplitude and phase. This amplitude, $\Delta B_{pu}^{n=1}$, measured by an array of 12 poloidal field sensors above the device midplane, includes both the RWM field as well as the field generated by mode-induced eddy currents in the passive stabilizing plates. The amplitude modulation shown in FIG. 1(d) is attributed to the interaction of the mode and eddy current fields. The field generated by I_A is compensated from $\Delta B_{pu}^{n=1}$. Comparison of the plasmas with and without active stabilization shows $\Delta B_{pu}^{n=1}$ is larger in the non-stabilized plasma as the n = 1 RWM becomes unstable, and is controlled at an average level of about 5 G in the stabilized plasma. During n = 1 stabilization, the n = 2

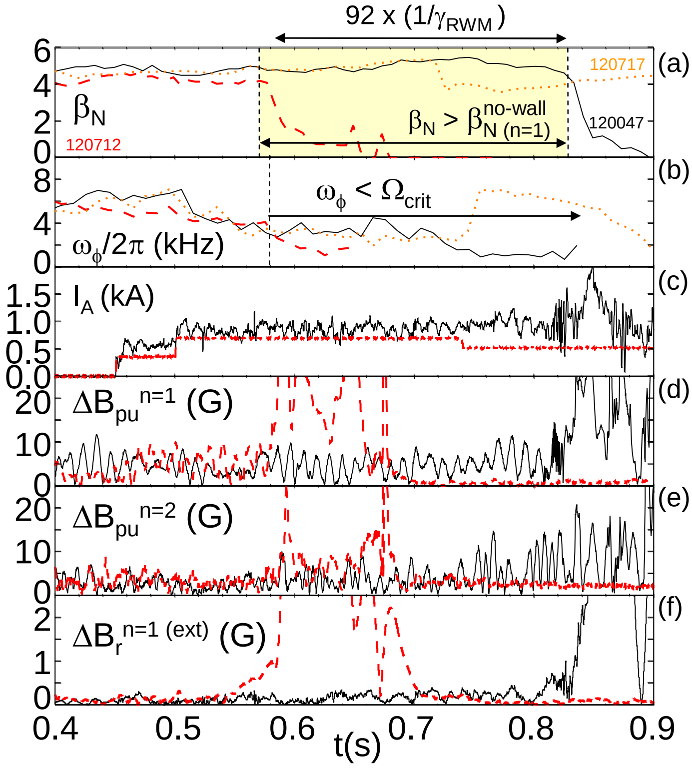

FIG. 1. RWM active feedback stabilization in low rotation plasmas. Solid curves: actively stabilized plasma at ω_ϕ significantly below Ω_{crit}, dashed curves: RWM unstable plasma at $\omega_\phi/\Omega_{crit}$ = 1 with active feedback turned off, dotted curves: (upper two frames) actively stabilized plasma suffering a beta collapse from an internal n *= 2 plasma mode. Shown are the evolution of (a) β_N, (b) ω_ϕ near* q *= 2, (c) current in representative non-axisymmetric control coil, (d) and (e) mode amplitude of* n *= 1 and 2 field components measured by the upper* B_p *sensor array, and (f) mode amplitude of* n *= 1 field component at the midplane, external to the vacuum vessel.*

RWM does not become unstable, although $\Delta B_{pu}{}^{n=2}$ becomes larger than $\Delta B_{pu}{}^{n=1}$ at the lowest values of ω_ϕ and highest values of β_N (FIG. 1(e)). The actively stabilized, low ω_ϕ plasmas can suffer partial β_N collapses due to largely internal modes, which do not disrupt the plasma current, allowing β_N to recover. An example is shown by the dotted curves in FIG. 1. DCON calculations show that $\beta_N > \beta_{N(n=2)}{}^{no\text{-}wall}$ in the actively stabilized plasma, and the computed mode can be internal. Further detail of this mode will be discussed below. Along with the drop in β_N, plasma momentum is transported from the plasma core outward. The ω_ϕ profile continues to decrease to very low values in this plasma as β_N recovers.

3. RWM Detection and Plasma Rotation Control

The reconstructed equilibrium at peak β_N of the actively stabilized, low rotation plasma in FIG. 1, along with the positions of the copper stabilizer plates, RWM sensors, and mode control coils are shown in FIG. 2. There are 48 toroidally segmented stabilizer plates, covered with carbon tiles on the plasma facing side, and arranged symmetrically in four toroidal rings, two above and two below the device midplane. The plates are independently connected to the stainless steel vacuum vessel by high resistance supports. Magnetic loops measuring the radial, B_r, and poloidal, B_p, flux are located at each of the plates closest to the midplane, the B_r sensors mounted between the carbon tiles and the copper shells, and the B_p sensors mounted a few centimeters below each plate. The sensors are instrumented to detect modes with frequencies up to 2.5 kHz. There are 6 toroidally-conformed, two-turn control coils mounted close to the machine vacuum vessel. This configuration is similar to midplane port module coil designs for ITER. Each coil nominally covers 60 degrees of toroidal angle. In these experiments, the coils are powered independently in three diametrically-opposed pairs producing odd parity fields.

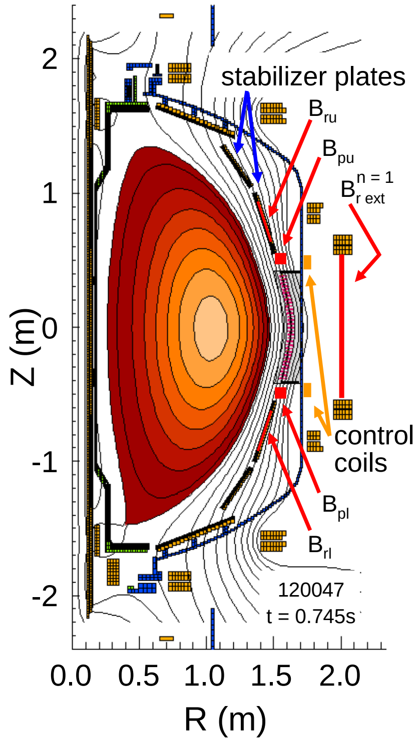

FIG. 2. Actively stabilized plasma equilibrium. Shown are the NSTX cross-section with poloidal flux contours, RWM sensor positions, and control coil locations.

Plasma toroidal rotation profiles for several plasmas are shown in FIG. 3 at various times of interest. For comparison to studies of DIII-D and ITER, ω_ϕ is normalized to $\omega_A \equiv B_{axis}/(R_{axis}(\mu_0\rho)^{0.5})$ where B_{axis} and R_{axis} are the magnetic field at, and major radial position of, the magnetic axis and ρ is the local plasma mass density. The profile with a peak value of $\omega_\phi / \omega_A = 0.325$ is from a typical rotationally stabilized plasma with $\beta_N > \beta_N{}^{no\text{-}wall}$. The profile with a peak value of $\omega_\phi/\omega_A = 0.125$ is from the plasma with no active stabilization in FIG. 1 at the time of RWM destabilization. It therefore defines the Ω_{crit}/ω_A profile. Note that at $q = 2$, $\Omega_{crit}/\omega_A = 0.038$, compared to a value of 0.02 in DIII-D, consistent with the observed dependence of Ω_{crit}/ω_A on aspect ratio (Ref [10], Fig. 15). The significantly reduced rotation profile of the actively stabilized plasma shown has $\omega_\phi/\Omega_{crit} = 0.2$ at $q = 2$. Also note that $\omega_\phi/\Omega_{crit} = 0.3$ at the magnetic axis. Comparing to predicted plasma rotation and critical rotation speeds for ITER advanced Scenario-4 plasmas [9], on-axis values are used, since a $q = 2$ surface does not exist in this ITER equilibrium. Ref. 9 states that $\omega_\phi/\omega_A = 0.018$, and that $0.015 < \Omega_{crit}/\omega_A < 0.03$ at the magnetic axis in ITER. Therefore, $1.2 < \omega_\phi/\Omega_{crit} < 0.6$ on axis in ITER, and so the actively stabilized plasma in NSTX has $\omega_\phi/\Omega_{crit}$ lower than ITER by at least a factor of 2. The ω_ϕ profile in FIG. 3 with the lowest values is taken from the actively stabilized plasma after the internal mode-induced β_N collapse and recovery FIG. 1. At this very low rotation level, two local regions in the profile have gone to zero rotation, most likely due to radially localized resistive modes electromagnetically locking to the stationary device error fields.

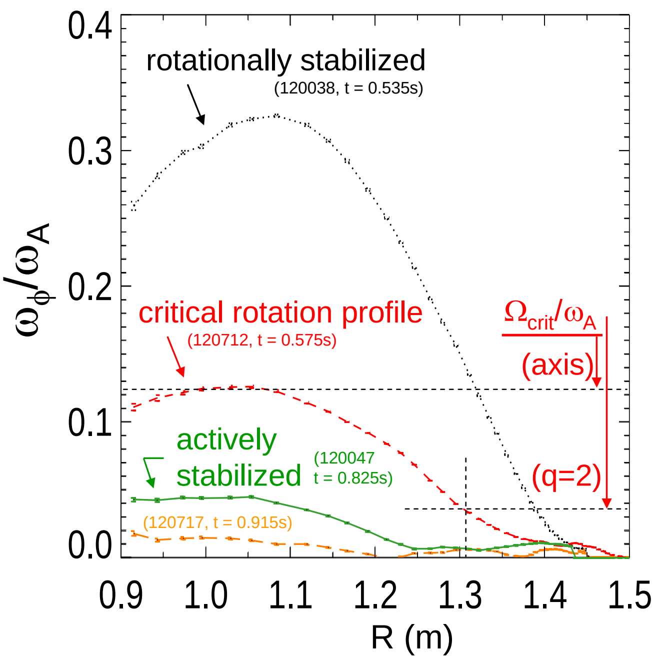

FIG. 3. Plasma rotation profiles for plasmas that are rotationally stabilized, are at RWM marginal stability (critical rotation profile), and are actively stabilized below Ω_{crit}.

4. RWM Control System and Parameter Variation

Variation of feedback control parameters for the active stabilization system demonstrated both positive and negative feedback response to the mode. The measured $n = 1$ RWM amplitude and phase, $\Delta B_{pu}{}^{n=1}$ and $\phi_{Bpu}{}^{n=1}$, are used to define the control coil currents,

$$I_A(\phi_{c(i)}, t) = G_p(t)\Delta B_{pu}^{n=1}(t)K_{c(i)}\cos(\phi_{c(i)} - \phi_{Bpu}^{n=1}(t) + \Delta\phi_f(t)) + I_{A0}(\phi_{c(i)}),$$

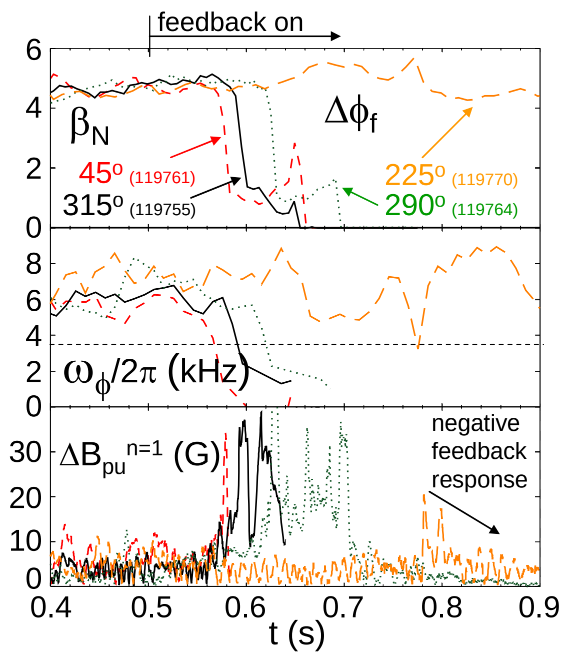

FIG. 4. Effect of feedback system relative phase on plasma stability. Various relative phases are depicted by different line styles.

where subscript i represents coil number, G_p and $\Delta\phi_f$ are time dependent gain and relative phase between the measured RWM amplitude and the control currents, $\phi_{c(i)}$ is the spatial toroidal offset for each of the control coils, $K_{c(i)}$ are calibration factors for each control coil, set to 69 A/G, and $I_{A0}(\phi_{c(i)})$ are time-dependent currents that do not depend on the measured RWM. The $\phi_{c(i)}$ are chosen to create a dominantly $n = 1$ magnetic field for the feedback control. The $I_{A0}(\phi_{c(i)})$ are chosen to create the $n = 3$ braking field. The effect of varying the relative phase $\Delta\phi_f$ on the plasma is shown in FIG. 4 at $G_p = 1.0$. Choosing $\Delta\phi_f$ constant for each discharge, and varying from 45 degrees through smaller angles, $\Delta B_{pu}{}^{n=1}$ shows a positive feedback response for angles through 290 degrees. At $\Delta\phi_f = 45$ degrees, the RWM is driven unstable soon after the feedback stabilization system is turned on. With an unfavorable relative phase, $\Delta B_{pu}{}^{n=1}$ increases, leading to lower ω_ϕ, which in turn increases $\Delta B_{pu}^{n=1}$ if $\beta_N > \beta_N^{no\text{-}wall}$, creating positive feedback, RWM instability, β_N collapse, and plasma current disruption. As $\Delta\phi_f$ is decreased, RWM instability is delayed, until at $\Delta\phi_f$ = 250 degrees (same result at 225 degrees), the plasma is actively stabilized. The plasma with $\Delta\phi_f$ = 225 degrees suffers a partial β_N collapse due to an internal mode at t = 0.765s. A damped response to this mode is observed in $\Delta B_{pu}^{n=1}$, indicating that control parameters are favorably set to produce negative feedback. The proportional gain G_p was also varied between 0.7 – 2.0 at $\Delta\phi_f$ = 225 degrees. Values up to G_p = 1.5 produced negative feedback, while equal or greater values resulted in a high frequency instability in the feedback control loop.

RWM stabilization can fail due to a change in the poloidal form of the mode. An example is shown in FIG. 5, where the n = 1 components of both upper and lower B_p and B_r sensors, and $\Delta B_{r\text{-}ext}^{n=1}$ sensor signals are shown. Note that since the latter sensor is outside the vacuum vessel, signals lag those of the internal sensors by ~ O(τ_w) ~ 6 ms for n = 1. Approaching the time of β_N collapse, $\Delta B_{pu}^{n=1}$ and $\Delta B_{pl}^{n=1}$ first decrease to near zero, as the radial field sensors increase by a small amount. Then, $\Delta B_{pu}^{n=1}$ increases strongly, while $\Delta B_{pl}^{n=1}$ lags, and the ratio $\Delta B_{pl}^{n=1}/\Delta B_{pu}^{n=1}$ never gets above 0.5. There is also a strong increase in $\Delta B_{r\text{-}ext}^{n=1}$ while $\Delta B_{ru}^{n=1}$ and $\Delta B_{rl}^{n=1}$ decrease, indicating that the mode is bulging through the midplane gap in the stabilizing plates and decreasing in amplitude in front of the plates. This observation may indicate a lack of "mode ridigity", normally assumed theoretically and observed experimentally [14]. Note that similar behavior is observed under passive stabilization alone, indicating that the stabilizing plate geometry may be partially responsible. The result has applicability to future devices with similar passive plate geometry, such as KSTAR. This poloidal deformation appears to occur when large control currents are requested and sometimes when the central q is near unity. These conditions may lead to nearby stable n = 1 MHD modes becoming less stable, causing the primary RWM eigenfunction to change poloidal structure.

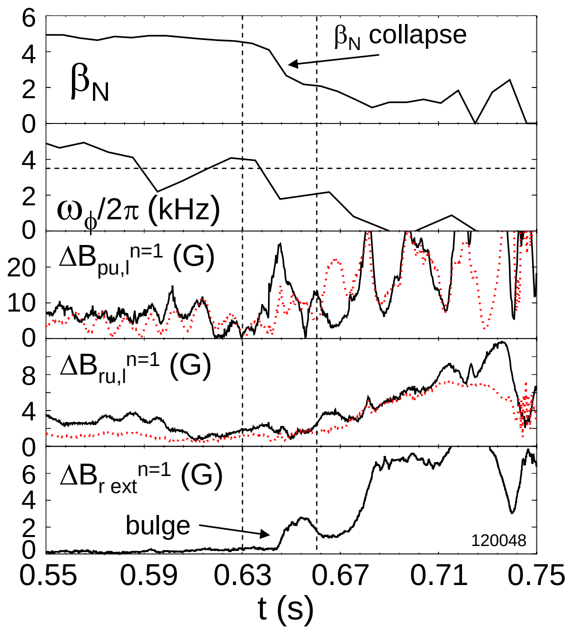

FIG. 5. Poloidal deformation leading to mode destabilization. Sensors are distinguished by solid lines (upper sensors) and dotted lines (lower sensors).

5. Mode Activity During *n* = 1 RWM Active Stabilization

Further detail of the measured n = 1 and 2 RWM amplitude and phase, along with chord integrated soft X-ray (SXR) measurements spanning from the plasma core to the edge [25] are shown in FIG. 6. Without active stabilization (FIG. 6(a)), the n = 1 RWM is the primary instability leading to the β_N collapse. At early times in the figure, $\phi_{Bpu}^{n=1}$ appears to wobble between 150 and 300 degrees, eventually settling to the lower end of this range, and as $\Delta B_{pu}^{n=1}$ grows exponentially, $\phi_{Bpu}^{n=1}$ shows mode rotation in the direction of plasma rotation, as expected by theory. SXR data shows the mode amplitude largest in the outer region of the plasma, propagating toward the core during mode growth. The n = 2 RWM amplitude will show periods when $\Delta B_{pu}^{n=2} > \Delta B_{pu}^{n=1}$, but the n = 2 mode growth that eventually occurs,

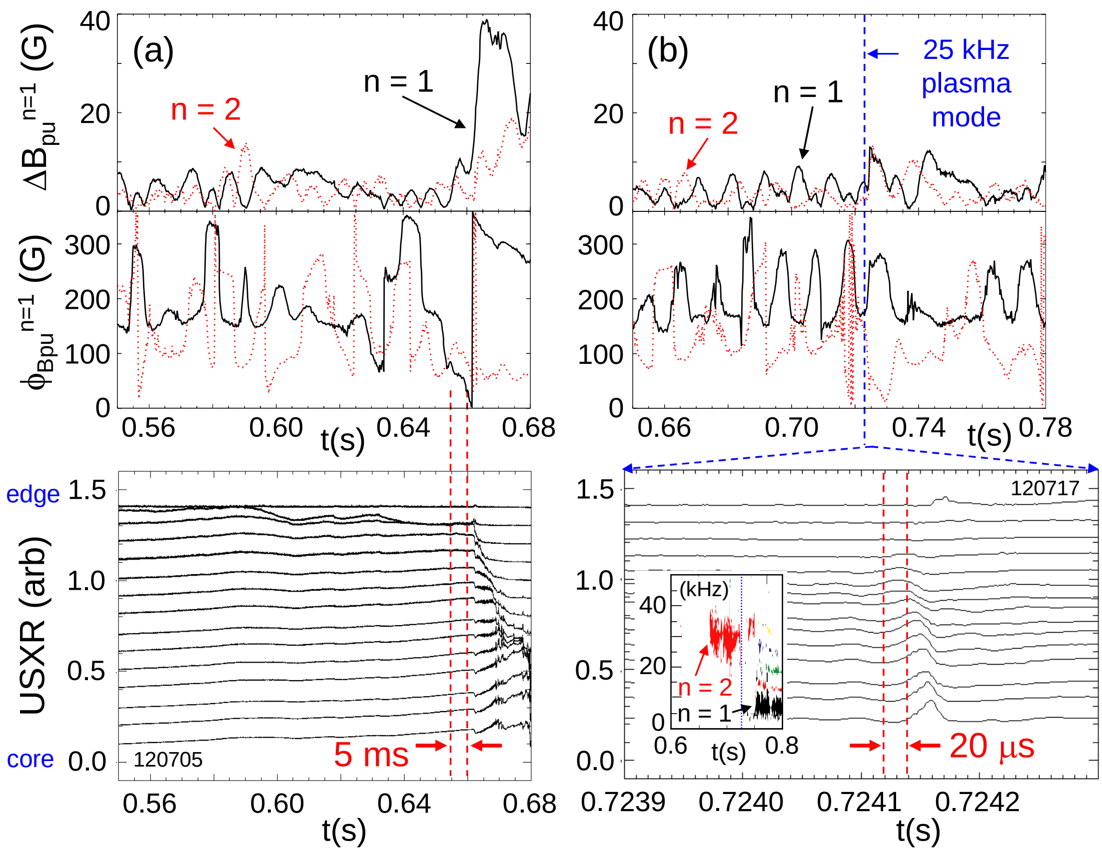

FIG. 6. Mode activity in plasmas with and without active stabilization. Frames from top down show upper B_p *sensor amplitude, phase, and ultra-soft X-ray emission spanning from the plasma core to edge vs. time. Solid lines:* n = 1*, dotted:* n = 2*. Column (a) discharge with active feedback off, column (b) RWM actively stabilized plasma with internal* n = 2 *plasma mode. Lower frame inset:* n *spectrum from midplane toroidal magnetic pickup coil array.*

although strong, is subsidiary to n = 1 mode growth. FIG. 6(b) shows analogous detail for the actively stabilized plasma suffering a largely internal mode shown in FIG. 1. Both n = 1 and 2 RWM activity is stable, with $\phi_{Bpu}^{n=1,2}$ wobbling within some range. SXR data shows the mode to grow on an ideal MHD timescale, much faster than τ_w, is largely internal, and the measured 25 kHz frequency indicates that the mode is n = 2, since it appears in a region of the plasma with $\omega_\phi/2\pi$ ~ 12 - 15 kHz. The n spectrum measured by a toroidal array of magnetic pickup loops also shows n = 2 mode activity at this frequency and time. DCON stability calculations are consistent with the identification of this mode as an n = 2 internal MHD instability.

6. Conclusion

The first RWM active stabilization experiments in low aspect ratio tokamak plasmas have demonstrated n = 1 RWM stabilization at low plasma rotation with direct applicability to future burning plasma experiments, including ITER. Stabilization of the n = 1 RWM did not lead to n = 2 destabilization. Under certain conditions, the mode is observed to deform poloidally, allowing destabilization. This may be due to the present combination of the stabilizing plate geometry and the location of sensors used for stabilization. Further study will assess the effect of various sensor combinations (using $\Delta B_{pu,l}^{n=1}$ and $\Delta B_{ru,l}^{n=1}$) on active RWM stabilization performance.

This research was supported by the U.S. Department of Energy under contracts DE-FG02-99ER54524 and DE-AC02-76CH03073.

References

[1] SABBAGH, S.A., BELL, R.E., MENARD, J.E., et al., Phys. Rev. Lett. **97** (2006) 045004.
[2] BONDESON, A., and WARD, D.J., Phys. Rev. Lett. **72** (1994) 2709.
[3] STRAIT, E.J., TAYLOR, T.S., TURNBULL, A., et al., Phys. Rev. Lett. **74** (1995) 2483.
[4] GAROFALO, A.M., STRAIT, E.J., JOHNSON, L.C., et al., Phys. Rev. Lett. **89** (2002) 235001.
[5] SABBAGH, S.A., SONTAG, A.C., BIALEK, J.M., et al., Nucl. Fusion **46** (2006) 635.
[6] GAROFALO, A.M., JENSEN, T.H., STRAIT, E.J., et al., Phys. Plasmas **10** (2003) 4776.
[7] CHU, M.S., GREENE, J.M., JENSEN, T.H., et al., Phys. Plasmas **2** (1995) 2236.
[8] GAROFALO, A.M., TURNBULL, A.D., AUSTIN, M.E., et al., Phys. Rev. Lett. **82** (1999) 3811.
[9] LIU, Y., BONDESON, A., CHU, M.S., et al., Nucl. Fusion **45** (2005) 1131.
[10] REIMERDES, H., HENDER, T.C., SABBAGH, S.A., et al., Phys. Plasmas **13** (2006) 056107.
[11] SONTAG, A.C., SABBAGH, S.A., ZHU, W., paper EX/7-2Rb submitted to this conference.
[12] SHIMADA, M., MUKHOVATOV, V., FEDERICI, G., et al., Nucl. Fusion **44** (2004) 350.
[13] GAROFALO, A.M., CHU, M.S., FREDRICKSON, E.D., et al., Nucl. Fusion **41** (2001) 1171.
[14] OKABAYASHI, M., BIALEK, J.M., CHANCE, M.S., et al., Phys. Plasmas **8** (2001) 2071.
[15] STRAIT, E.J., BIALEK, J.M., BOGATU, I.N., et al., Phys. Plasmas **11** (2004) 2505.
[16] BRUNSELL, P.R., YADIKIN, D., GREGORATTO, D., et al., Plasma Phys. Control. Fusion **47** (2005) B25.
[17] GAROFALO, A.M., JENSEN, T.H., STRAIT, E.J., et al., Phys. Plasmas **9** (2002) 4573.
[18] PENG, Y.-K.M. and STRICKLER, D., Nucl. Fusion **26** (1986) 769.
[19] KAYE, S.M., BELL, M.G., BELL, R.E., et al., Nucl. Fusion **45** (2005) S168.
[20] ZHU, W., SABBAGH, S.A., BELL, R.E., et al., Phys. Rev. Lett. **96** (2006) 225002.
[21] LEE, G.S., KWON, M., DOH, C.J., et al., Nucl. Fusion **41** (2001) 1515.
[22] BIALEK, J.M., BOOZER, A.H., MAUEL, M.E., et al., Phys. Plasmas **8** (2001) 2170.
[23] SABBAGH, S.A., KAYE, S.M., MENARD, J.E., et al., Nucl. Fusion **41** (2001) 1601.
[24] GLASSER, A.H. and CHANCE, M.C., Bull. Am. Phys. Soc. **42** (1997) 1848.
[25] STUTMAN, D., FINKENTHAL, M., MOOS, H.W., et al., Rev. Sci. Instrum **74** (2003) 1982.